ROYAL SOCIETY
OF CHEMISTRY

PAPER

Check for updates

The phase behavior of CO_2 injection in shale reservoirs with nano-pores

Tao Wan, [ID] *[a] Kun Ding,[b] Qiyong Xiong[b] and Jing Guo[c]

The main purpose of this paper is to study the solubility of CO_2 in oil and water phase under high temperature and pressure. Firstly, CO_2-crude oil PVT experiments were carried out to determine the physical parameters of the reservoir fluid in the study field in order to clarify the interaction mechanism of CO_2 with the crude oil. Secondly, the solubility of CO_2 in the reservoir fluid under different pores and the minimum mixed-phase pressure of the CO_2-crude oil system were calculated by the improved Peng–Robinson equation of state. In this paper, the effects of nano-pores limitation on CO_2 solubility were studied. The results show that pressure increase is favorable to CO_2 dissolution, the solubility increases with the increase of the oil–water ratio. CO_2 solubility decreases with temperature increase. The greater the mineralization of formation water, the lower the CO_2 solubility. Nanopore confinement causes the phase envelope to contract and the minimum mixed-phase pressure to decrease. When the pore radius is smaller, the restriction of the phase envelope is stronger. In this paper, the minimum mixing pressure of crude oil and carbon dioxide is reduced from 31.25 MPa at 50 nm to 21.25 MPa at 5 nm, thus it is beneficial for enhanced oil recovery (CO_2-EOR). Nanopore confinement favors CO_2 to enhance shale oil recovery. The results of this study are critical to evaluate the effect of CO_2 sequestration, solubility and phase behavior changes of CO_2 in shale reservoirs with nano-pores.

1 Introduction

Shale oil is mature oil stored in shale formations with nanometer pore size and rich with organic matter. Efforts have been made in recent decades to improve oil recovery of unconventional shale reservoirs. Gas injection is one of the most used methods for shale oil production because of its high displacement efficiency.[1,2] It is believed that CO_2 tends to adhere to the shale surface and therefore has a higher adsorption capacity in shale reservoirs.[3,4] CO_2 adsorption is key to improving CO_2 geological storage capacity. Previous studies have shown that reservoir fluids and reservoir thermodynamics affect CO_2 adsorption capacity.[5] Studies on the application of CO_2 gas injection to unconventional shale reservoirs have shown that cyclic CO_2 injection can greatly improve shale oil recovery rates.[6,7] Early studies have shown that shale reservoirs are potential places for geological storage of CO_2.[8] With a serious environmental impact and long-term detrimental effect on the atmospheric balance caused by CO_2 emissions in recent years, CO_2 enhanced oil recovery (EOR) and storage of CO_2 in the formation is undoubtedly an effective way to reduce carbon emissions. However, there are still many uncertainties

regarding CO_2 injection, such as complex phase behavior, hydraulic/natural fracture system, and geomechanically effects.

There are three mechanisms for CO_2 storage in saline aquifers: dissolution, mineralization, and gas capture. The literature shows that solubility trapping is more effective than mineralization. CCUS is one of the promising options for long-term storage of large quantities of CO_2. Too much dissolved CO_2 will change the chemical characteristics of the formation water. A previous study investigated the solubility of CO_2 in formation water. The solubility of CO_2 increased with the increase of pressure. When the temperature and pressure are constant, the solubility of CO_2 decreases with the increase of formation water salinity. Therefore, the solubility of CO_2 in aquifers is very important for the CCUS project.[9]

As the main recovery mechanism of CO_2 enhanced oil recovery (EOR) is miscibility, Welker (1963) studied the solubility of CO_2 in crude oil, and measured crude oil expansion factor and viscosity under different CO_2 injection amounts.[10] Results showed that the solubility of CO_2 in crude oil was very high. The expansion factor and solubility of CO_2 were positively correlated with pressure and negatively correlated with temperature. When crude oil has less heavy component contents, the solubility of CO_2 in it is greater. Viscosity reduction effect caused by CO_2 injection is more obvious when the viscosity of crude oil is higher. Therefore, the study on the solubility of CO_2 in crude oil has a certain guiding significance for CO_2 flooding enhanced oil recovery.

[a]Faculty of Petroleum, China University of Petroleum (Beijing) at Karamay, China. E-mail: 2017592002@cupk.edu.cn; Fax: +86990 6633510; Tel: +86990-6633531
[b]Xinjiang Oilfield Company, PetroChina, China
[c]China University of Petroleum (Beijing), China

The fluid phase changes with the change in temperature and pressure during reservoir production. Depending on formation temperature and pressure, CO_2 can be injected in gas, liquid or supercritical phases. Experimental testing of fluid PVT phase characteristics is an important step in the engineering design of CO_2 flooding and storage. Suo (2021) conducted a series of CO_2 displacement of water-saturated cores. The effect of different CO_2 phase state, purity and pore structure on residual water was investigated.[11] It is concluded that the larger viscosity of liquid CO_2 will reduce the diffusion coefficient and lead to a longer breakthrough time. The storage capacity will be larger when the liquid phase CO_2 is used for storage. The identification of the CO_2 phase is an important guiding for cap leakage monitoring, CO_2 effective storage evaluation, cap rock integrity.

The pore size of shales commonly ranges from 5 to 100 nm. The fluid phase behavior in the nano-pore of shales is complex, and the distribution of nano-pore sizes affects the phase equilibrium of the reservoir fluid, resulting in a reduction of the minimum miscible pressure (MMP). It has been pointed out that due to the nano-pore confining effect, the critical pressure and critical temperature of shale gas have changed, which is different from that of conventional formations. During gas injection process, phase equilibrium is crucial to determine the vapor–liquid equilibrium volume, swelling effect, gas solubility and minimum miscible pressure (MMP), where the influence of the nanoscale confining effect needs to be considered.[12]

The solubility of CO_2 in crude oil is inseparably connected to the phase behavior.[13] Therefore, it is of practical significance to study the phase behavior of reservoir fluid in nano pores during CO_2 flooding. The combination of equations of state and capillary pressure has been explored to explain the effect of nano confining on the behavior of the fluid phase.[14] The effects of nano pores, adsorption and diffusion on the condensate phase behavior were considered in the simulation process. Results showed that nano-confinement became significant when the pore size was less than or equal to 4 nm.

A survey of the literature found that pore geometry and wettability also affect fluid behavior. The porous medium of shale reservoirs is strongly non-homogeneous, and its pore geometry has a large impact on fluid transport. In conventional oil and gas reservoirs, the use of circular pore approximation to represent the pore type is reasonable in many applications, whereas in shale reservoirs, the pores have a large surface-to-volume ratio, and therefore fluid flow in shale systems depends more on the shape of the pores.[15]

Interfacial wettability affects the mass transfer process of a fluid in a solid–liquid phase transition, and a high degree of wettability promotes the mass transfer process. A change in the wetting angle affects the heat transfer process between the fluid and the solid. Stronger wettability means that the fluid is more likely to expand on the solid surface, which will change the flow pattern of the fluid.

1.1 Problem context and challenge

Most of the research on the solubility of CO_2 in oil–water systems remains in single-phase oil and water.[6] Nano-restriction effects lead to an inability to determine the phase behavior of reservoir fluids in shales under nano porosity.[16]

1.2 Research gap

In this study, we carried out indoor experiments and numerical simulations for the Jimsar shale oil field in Xinjiang, to investigate the solubility of CO_2 in formation fluids under different formation conditions as well as the phase changes, the oil repelling effect of CO_2 and the feasibility of CO_2 sequestration in shale reservoirs, so as to provide preliminary theoretical support for selecting a more efficient development method and sequestration site. And it can provide a basis or computational model for dissolution sequestration.

1.3 Main contributions

In this paper, the phase behavior of reservoir fluids are investigated by using four different oil samples. The solubility of CO_2 in reservoir fluids was simulated and fitted the experimental results. The critical properties of components are used to represent the phase behavior of reservoir fluids in nano-pores. CMG-Winprop simulator was used to model the influence of nano-pore sizes on the solubility and phase behavior of CO_2 during CO_2 injection.

The samples selected in this study are degassed crude oil from four horizontal wells in Jimsar Shale, Xinjiang. Since the large-scale development of Jimsar shale oil in 2018, the annual oil production of Jimsar shale oil has exceeded 500 000 tons. However, due to high oil viscosity, complex distribution of nano-pore size, and petrophysical heterogeneity among different crudes, the solubility and phase behavior experiments of CO_2–oil–water are carried out. The salinity of formation water in Jimsar is about 15000 mg L^{-1}. The reservoir temperature is about 80 °C, and the reservoir pressure is about 40 MPa. The properties of crude oil components used in this research are shown in Table 1. The physical properties of crude oil are shown in Table 2, and the chemical composition of formation water is shown in Table 3.

Table 1 Properties of degassed crude oil components in Jimsar shale oil

Components	MW	Composition			
		J41H	JHW07121	JHW5815	JHW051
CH_4	16.043	9×10^{-9}	9×10^{-9}	9×10^{-9}	9×10^{-9}
C_2H_6	30.07	9×10^{-9}	9×10^{-9}	9×10^{-9}	9×10^{-9}
C_3H_8	44.097	0.0056	0.0051	0.0167	0.0058
IC_4	58.124	0.0041	0.0237	0.0112	0.0047
NC_4	58.124	0.0122	0.0212	0.0218	0.0143
IC_5	72.151	0.0646	0.0443	0.0613	0.0504
NC_5	72.151	0.0550	0.0350	0.0439	0.0435
C_6	86	0.0600	0.0516	0.0579	0.0519
C_7–C_{11}	111.275	0.1325	0.1208	0.1418	0.1452
C_{12}–C_{19}	214.522	0.2426	0.2394	0.2199	0.2394
C_{20}–C_{29}	324.000	0.2423	0.2572	0.2333	0.2572
C_{30+}	609.365	0.1811	0.2017	0.1922	0.1876

Table 2 Physical properties of degassed crude oil from Jimsar shale oil

		JHW051	JHW5815	JHW07121	J41H
Density, (20 °C) g cm^{-3}		0.9037	0.9001	0.8934	0.8834
Viscosity, mPa s	20 °C	487	286	203	83.2
	80 °C	68.3	65.3	47.5	24.7

Table 3 Composition of formation water in Jimsar Depression

Water type	PH	HCO$_3^-$ (mg L^{-1})	Cl$^-$ (mg L^{-1})	SO$_4^{2-}$ (mg L^{-1})	Ca^{2+} (mg L^{-1})	Mg^{2+} (mg L^{-1})	Na$^+$ (mg L^{-1})	K$^+$ (mg L^{-1})
NaHCO$_3$	8.0	3527.68	1146.2	177.3	17.72	7.06	2124.53	7000.49

Fig. 1 Experimental equipment system.

2 Experiment and simulation

2.1 Experimental setup

The system shown in Fig. 1 was used in the experiment, which is composed of PVT cell determining phase behavior at high temperature and high-pressure, vacuum pumping system, PVT high-pressure viscometer, piston type accumulators, positive displacement pumps, syringe pump, gas sampling cylinder and gas flow meter. The experimental materials mainly used crude oil from four Lusaogou formation in Jimsar, ether, CO_2 and N_2, among this, ether and carbon dioxide and nitrogen with 99.99 percent purity.

2.2 Experimental procedures

Prior to conducting the experiments, the PVT instrument, pumps, accumulators and viscometer were cleaned with petroleum ether, and then dried with high-pressure nitrogen. The PVT chamber was vacuumed for 2 hours. Then, preheat the PVT instrument to formation temperature (80 °C). Crude oil was pumped into the PVT chamber by syringe pump. After stabilizing for a period of time, pressure, temperature and volume of fluid in the PVT chamber were recorded. CO_2 was subsequently transferred to the PVT cylinder by the syringe pump through accumulators. Specially designed magnetic stirrer was equipped with on top of piston. Rotate the PVT cell so that CO_2 can be fully dissolved in the crude oil.

(1) Constant expansion experiment: a sample of CO_2 dissolved reservoir fluid was placed in the PVT cell. Pressure of the PVT cell is raised above the formation pressure (40 MPa) to make sure that injected CO_2 was completely dissolved in the crude oil. Temperature was set to reservoir temperature (80 °C). The PVT cell volume was then increased resulting in a decreased pressure. The cell volume and pressure were measured at each step of pressure reduction (such as 5 MPa). No gas or liquid is removed from the cell.

(2) Flash vaporization: pressurize the PVT cell to the reservoir pressure, and measure the fluid volume of the PVT cell. Maintain the pressure of the PVT cell equal to initial reservoir pressure, and transfer a certain amount of CO_2–oil mixture from the PVT cell to the separator. Measure the volume and weight of released gas–oil mixture. Then calculate the bubble point pressure and gas–oil ratio.

(3) Viscosity measurement: PVT-viscometer was used to measure the high-pressure and high temperature reservoir fluids dissolved with CO_2. Firstly, the viscometer was heated to reservoir temperature, then a certain volume of fully mixed reservoir fluid sample was transferred to the viscometer.

After one set of experiments was completed, PVT cell and viscometers were cleaned up with petroleum ether. Then the experiments were repeated with different CO_2–oil ratios.

Table 4 Critical properties of each component at 5 nm

Components	P_c (atm)	T_c (K)	σ_{LJ} (nm)	P_{cp} (atm)	T_{cp} (K)
H_2O	217.6	647.3	0.350918	192.822	605.3251
CO_2	72.8	304.2	0.393006	63.74146	282.1565
CH_4	45.4	190.6	0.393622	39.74393	176.7672
C_2H_6	48.2	305.4	0.451506	41.51408	280.0533
C_3H_8	41.9	369.8	0.504244	35.56285	335.6185
IC_4	36	408.1	0.548123	30.18759	367.1906
IC_5	33.4	460.4	0.585041	27.72501	411.2354
C_6	32.46	507.5	0.610125	26.76041	451.0572
$C_7–C_{11}$	28.377	577.772	0.666272	23.03898	507.8091
$C_{12}–C_{19}$	17.716	726.245	0.841323	13.71539	616.2318
$C_{20}–C_{29}$	12.40	822.449	0.987692	9.224989	677.3358
C_{30+}	8.678	913.673	1.150851	6.189957	726.9363

Fig. 3 Variation of carbon dioxide solubility with critical temperature.

where f_i denotes the fugacity of the component.

Due to the nano-pore confining effect, the critical pressure and critical temperature of fluids in the pores have changed, which is different from that of conventional formations. In the simulation process, the change of fluid components' critical properties was calculated by the correlations used by Lopez *et al.* (2018).[17] The change of critical temperature was calculated by the correlation proposed by Zarragoicoechea and Kuz.[18] The relative critical temperature shift with the quadratic ratio of the Lennard-Jones collision diameter to the throat radius:

$$\Delta T_c = \frac{T_{cb} - T_{cp}}{T_{cb}} = 0.9409 \frac{\sigma_{LJ}}{r_{p35}} - 0.2415 \left(\frac{\sigma_{LJ}}{r_{p35}} \right)^2$$

where ΔT_c is the critical temperature deviation; T_{cb} is the critical temperature in the normal aperture state; T_{cp} is the critical temperature confined by the aperture; r_{p35} is the pore throat radius in nm;

σ_{LJ} is the Lennard-Jones (LJ) collision diameter which was calculated based on the volumetric critical properties of each component:

$$\sigma_{LJ} = 0.244^3 \sqrt{\frac{T_{cb}}{P_{cb}}}$$

P_{cb} and T_{cb} are the critical pressure and critical temperature of each component in normal state, respectively. The critical pressure change simulation was improved:

$$\Delta P_c = \frac{P_{cb} - P_{cp}}{P_{cb}} = 1.5686 \left(\frac{2r_{p35}}{\sigma_{LJ}} \right)^{-0.783}$$

where ΔP_c is the critical pressure deviation, P_{cp} is the critical pressure in nano-pores, and P_{cb} is the critical pressure at the normal aperture state. The critical properties of the components confined at 5 nm calculated by preceding method was presented in Table 4.

The critical nature of the components affects the solubility of carbon dioxide in the fluid, and the Fig. 2 and 3 show the variation of carbon dioxide solubility with the critical temperature and critical pressure of the fluid components respectively.

Fig. 2 Variation of carbon dioxide solubility with critical pressure.

2.3 Simulation

CMG-Winprop can simulate the solubility of CO_2 in oil and water phases with different levels of salinity and perform thermodynamic calculations. The mineralization of formation water is expressed by the NaCl concentration, Units of formation water can be specified prior to the calculation. The Henry's law constant is a function of pressure, temperature, and salinity, there are two correlations in Winprop to calculate the Henry's law constant, the correlation chosen for this chapter is the Harvey method. The Henry's constant for CO_2 is calculated as follows:

$$\ln H_i = \ln H_i^* + \frac{\bar{v}_i (P - P^*)}{RT}$$

where H_i^* denotes the Henry's constant for component 'i' at reference pressure and temperature, and $\bar{v}_i$ denotes the offset molar volume of component 'i'.

From the above, the definition of the fugacity coefficient can be introduced, the fugacity coefficient is an uncaused quantity that measures the degree of fugacity offset pressure of a real fluid. From this, combined with Henry's law, the solubility of the gas component in the aqueous phase can be expressed as:
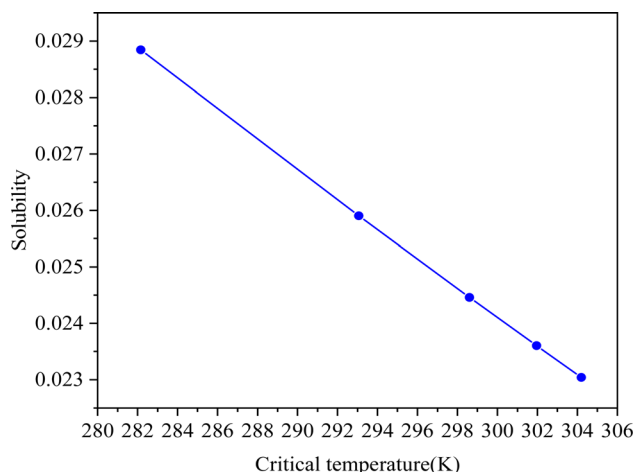
$$x_i = f_i / H_i$$

3 Results and discussion

3.1 Phase behavior of reservoir fluid-CO_2 by PVT test

Shale oil samples presented in Table 1 was used to investigate the phase behavior of CO_2–oil interaction. Four oil samples from Xinjiang shale oil reservoirs were used for CO_2–oil–water phase behavior in the experimental processes, as shown in Fig. 4. CO_2 dissolved in crude oil can significantly change the properties of the crude oil, especially oil formation volume and viscosity, which can reduce the flow resistance of crude oil. In this paper, different CO_2–oil ratios were conducted to measure the changes in crude oil viscosity, expansion factor, bubble point pressure and oil density.

Fig. 5 shows the relationship of fluids volume variations with pressure at different gas–oil ratios when oil saturation is 100%. Fig. 6 shows the relationship between relative volume and pressure at different oil saturations. It can be seen from Fig. 5

Fig. 4 Shale oil from Xinjiang were used in the experimental processes.

(a)J41

(b)JHW07121

(c)JHW5815

(d)JHW051

Fig. 5 $P–V$ relationship under different gas–oil ratios for different wells: (a) J41, (b) JHW07121, (c) JHW5815, (d) JHW051.

Fig. 6 The relationship between relative volume and pressure under different oil saturation: (a) J41, (b) JHW5815.
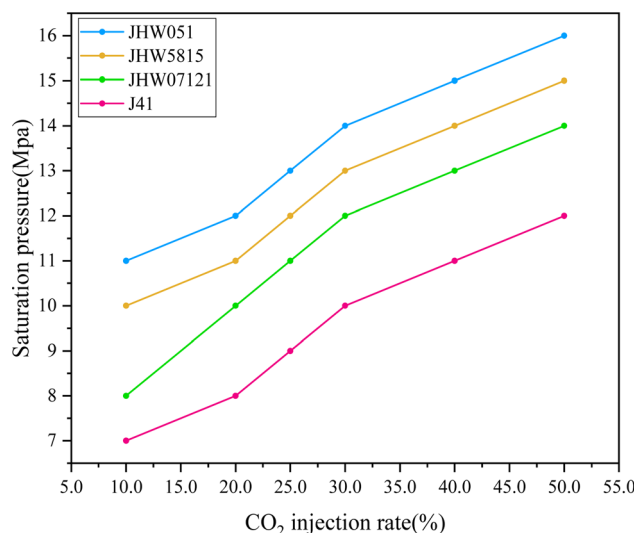

Fig. 7 Saturation pressure of CO_2–crude oil system changes with CO_2 injection.

that with the increase of gas–oil ratio, the bubble point pressure of crude oil continues to rise. From Fig. 6, it is observed that the bubble point pressure is decreased with an increase of oil saturation. The rationale behind this is that is more preferably dissolved in oil than water, thus fluid with a lower oil saturation has a higher bubble point pressure.

Fig. 7 shows the variation of saturation pressures of the CO_2–crude oil system with the amount of CO_2 injection. It can be seen that the saturation pressure of the well JHW051 shale oil–CO_2 system is the highest, indicating that CO_2 is more easily separated to form gas–liquid two phases in the production process of this well. That is because the viscosity of JHW051 oil is the heaviest, the saturation pressure is greater, and the solubility of CO_2 in crude oil is smaller. The viscosity of J41 is

the smallest, meanwhile the saturation pressure is the smallest. The ratio of light components to heavy components is high for crude oil of J41, which makes it easier for CO_2 to form miscibility with oil. It can be seen from these four wells that with the increase of CO_2 injection volume, the saturation pressures of the system also increase.

Fig. 8 shows the variation of crude oil expansion coefficient with CO_2 injection volume. As can be seen from the figure, the expansion coefficient of crude oil increases with the increase of CO_2 injection volume. The crude oil expansion coefficient of J41 is the largest, and that of JHW051 is the smallest. It suggests that CO_2 has a strong expansion capacity in crude oil, and the expansion factor is nearly twice after CO_2 injection.

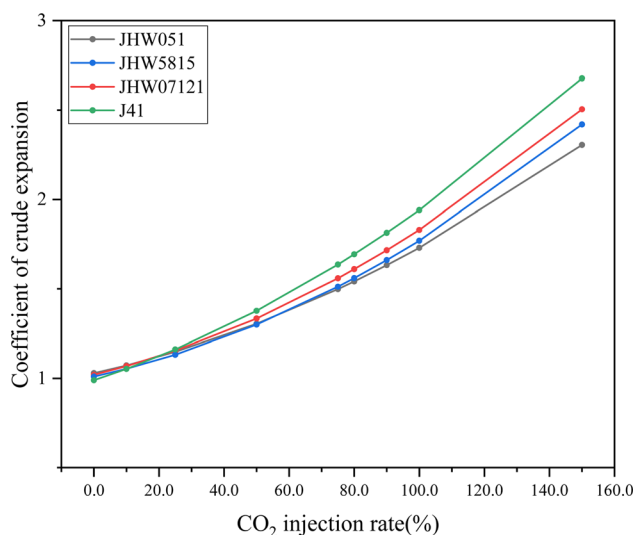Fig. 9 shows the change of crude oil viscosity with the amount of CO_2 injection. As can be seen from the figure, CO_2

Fig. 8 Variation of crude oil expansion coefficient with CO_2 injection volume.
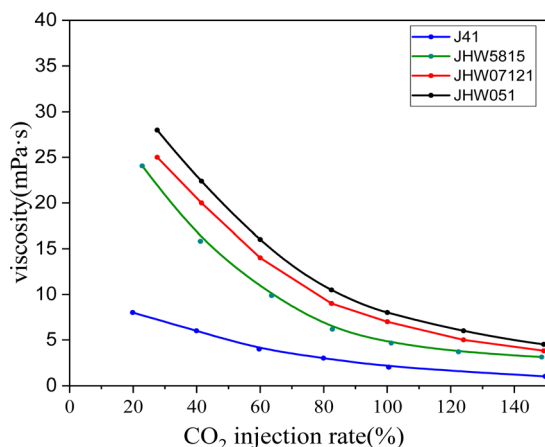
Fig. 9 Variation of crude oil viscosity with CO_2 injection.

injection has a renounced viscosity reduction effect in the early injection stage. After CO_2 injection exceeds 50% injection volume, the crude oil viscosity contains decrease, but the decline rate decreases with CO_2 injection. The viscosity of each crude oil decreased by more than 70%, It can be concluded that

CO_2 has a very good viscosity reduction effect on crude oil. As CO_2 is dissolved in the crude oil, the lighter components are extracted, which leads to a reduction in the viscosity of the crude oil. The decreasing trend of J41 crude oil viscosity is gentler due to the fact that J41 crude oil has a higher content of lighter components, and is more miscible with CO_2.

Crude oil components of Jimsar shale oil in Table 1 was used to simulate the phase behavior with CO_2 injection. CMG's WINPROP was employed to calculate the phase behavior and fluid properties of the flowing fluid at reservoir temperature and pressure. Fig. 10 shows the comparing results of numerical simulation with experimental results. It is seen that the regression values of the relative volume have good agreement with the experimental values, and the overall deviations are less than 5%.

3.2 Solubility change of CO_2 under conventional conditions

3.2.1 Solubility analysis of CO_2 in water. Before the experiment, the PVT reactor and pipeline were cleaned with petroleum ether, dried with N_2, and finally vacuumed to remove all impurities. The temperature of PVT chamber was set to the formation temperature at 80 °C, so that the PVT reactor
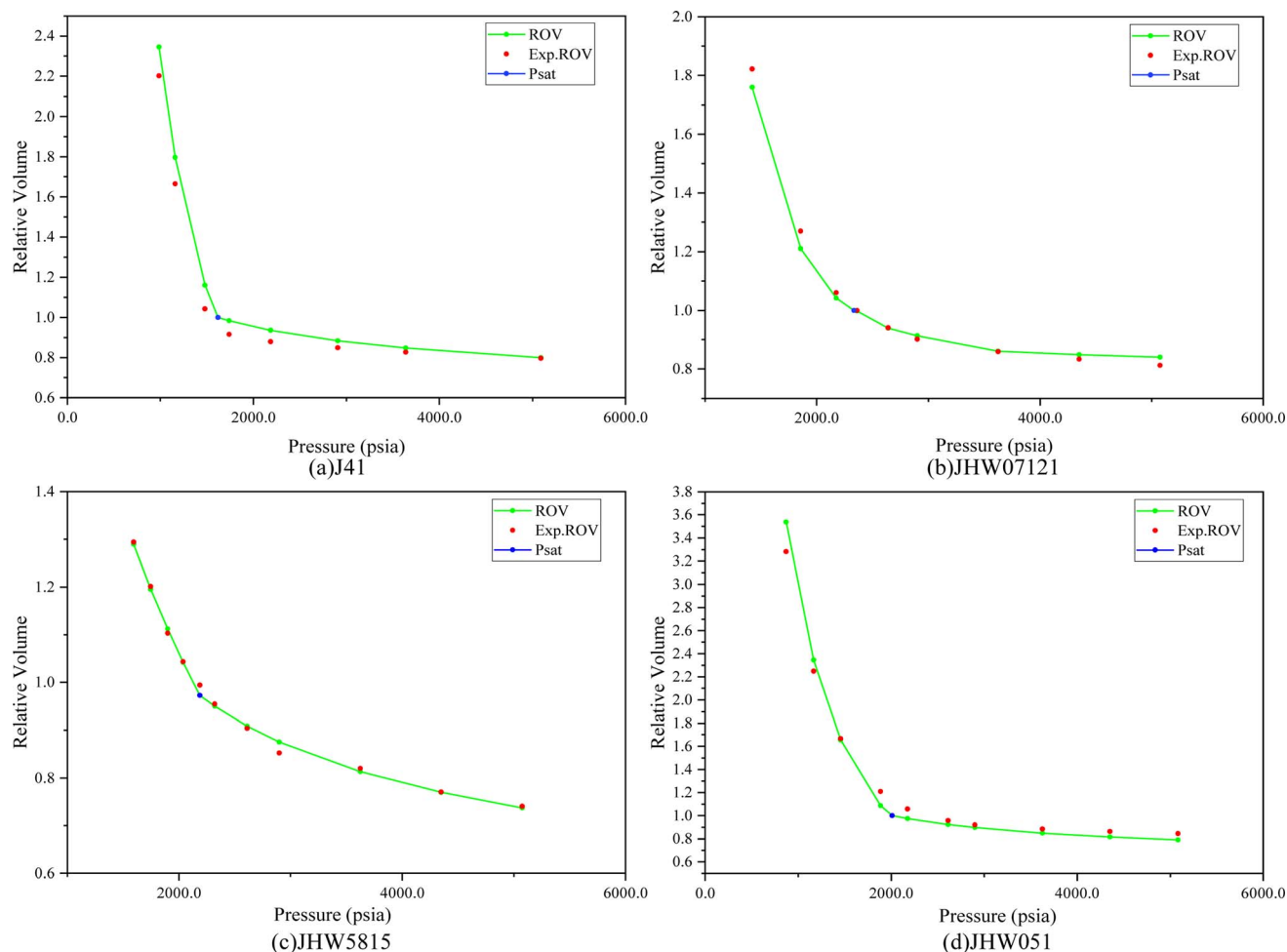

Fig. 10 Numerical model validation by regression with experimental results for different wells: (a) J41, (b) JHW07121, (c) JHW5815, (d) JHW051.
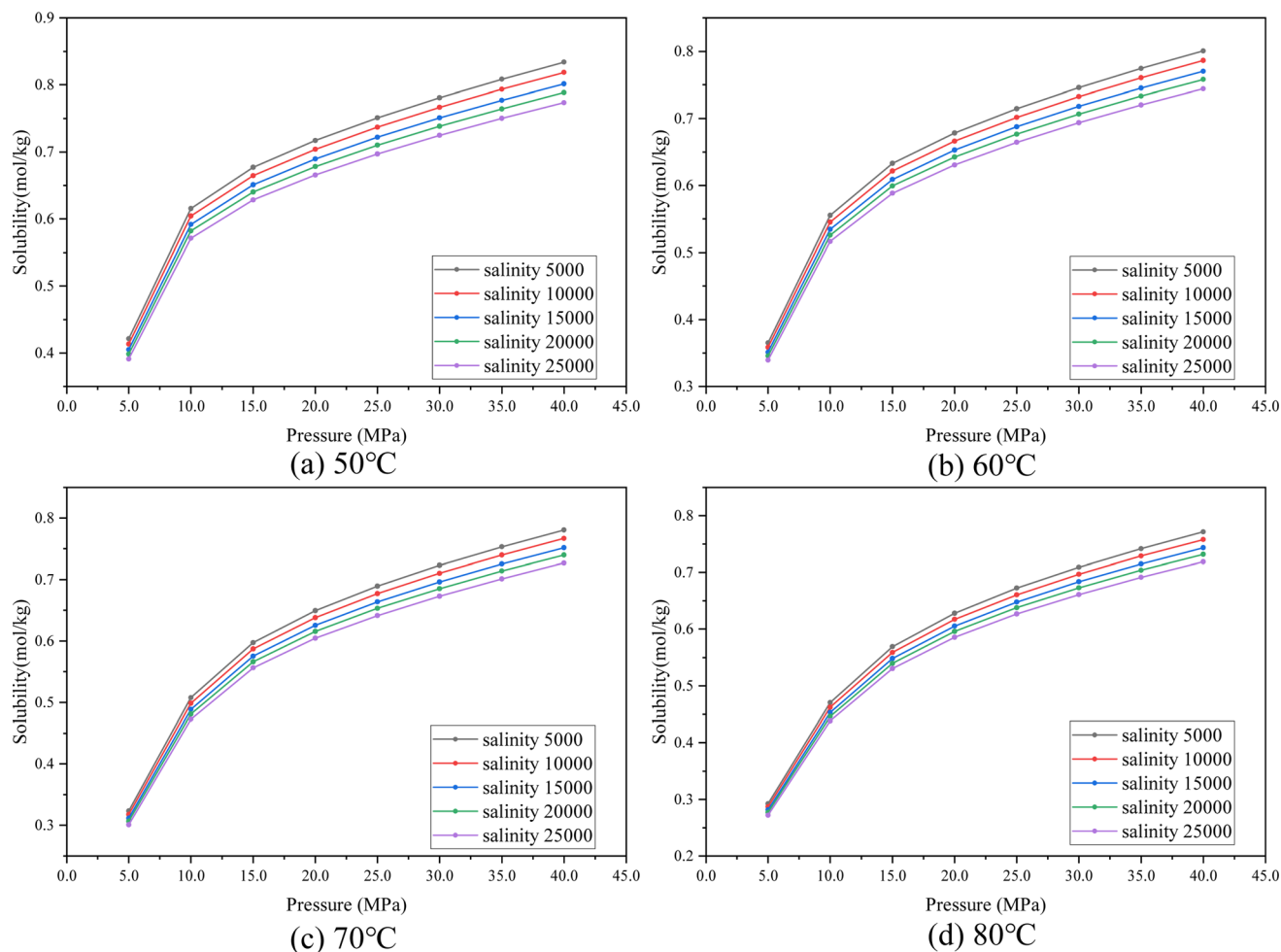
Fig. 11 The effect of salinity on CO_2 solubility in water at different temperatures: (a) 50 °C, (b) 60 °C, (c) 70 °C, (d) 80 °C.

temperature remained unchanged for 24 hours. To determine the solubility of CO_2 in crude oil, formation water, and their mixtures, CO_2 was first pumped into the PVT chamber, and the entire system pressure remained unchanged for 4 hours. Record the initial pressure P_0 and volume V_0. Then, use a high-pressure syringe pump to inject crude oil and formation water respectively to obtain the formation water–oil ratio.

After CO_2, oil and water injection process is completed, magnetic stirring is activated to ensure CO_2 was fully dissolved into the liquid system. The pressure of PVT chamber will continue to decrease as the dissolution proceeds. After the CO_2 gas and liquid phases reach equilibrium, stirring will be stopped. If the pressure no longer changes, record the equilibrium pressure P_e and corresponding equilibrium volume V_e. The liquid volume V_1 can be directly observed from the chamber.

$$C = \frac{1}{V_e}\left[\frac{P_0 V_0}{RTZ_0} - \frac{P_e(V_e - V_1)}{RTZ_e}\right]$$

where V_e is the volume of fluids at equilibrium; V_1 represents the volume of liquid at equilibrium; $V_e - V_1$ is the volume of gaseous CO_2 at equilibrium; P_0 represents the pressure of CO_2 at initial

condition; P_e is the pressure at equilibrium condition; Z_0 represents the Z factor of CO_2 at initial condition; Z_e represents the Z factor of CO_2 at equilibrium.

Fig. 11 shows the change of the solubility of CO_2 at different water salinity from 5000 to 25 000 mg L^{-1} at different temperatures. When the temperature and the mineralization of the water are kept constant, the solubility of CO_2 in water shows a gradual increase with increasing pressure, but the magnitude of the increase in CO_2 solubility gradually decreases.

Fig. 12 shows the change of solubility of CO_2 with temperature in water with a salinity from 5000 to 25 000 mg L^{-1}. As you can see from the graph, when the pressure and mineralization are certain, the solubility of CO_2 shows a gradual decrease with increasing temperature; when the pressure and temperature are constant, the solubility of CO_2 in water decreases with increasing mineralization. With the increasing temperature, the magnitude of the change of CO_2 solubility with temperature also decreases gradually. When the temperature and pressure were kept constant, the solubility of CO_2 decreased with the increase of water mineralization, and the greater the pressure, the greater the difference in the solubility of CO_2 in the water of different mineralization strata, indicating that the effect of
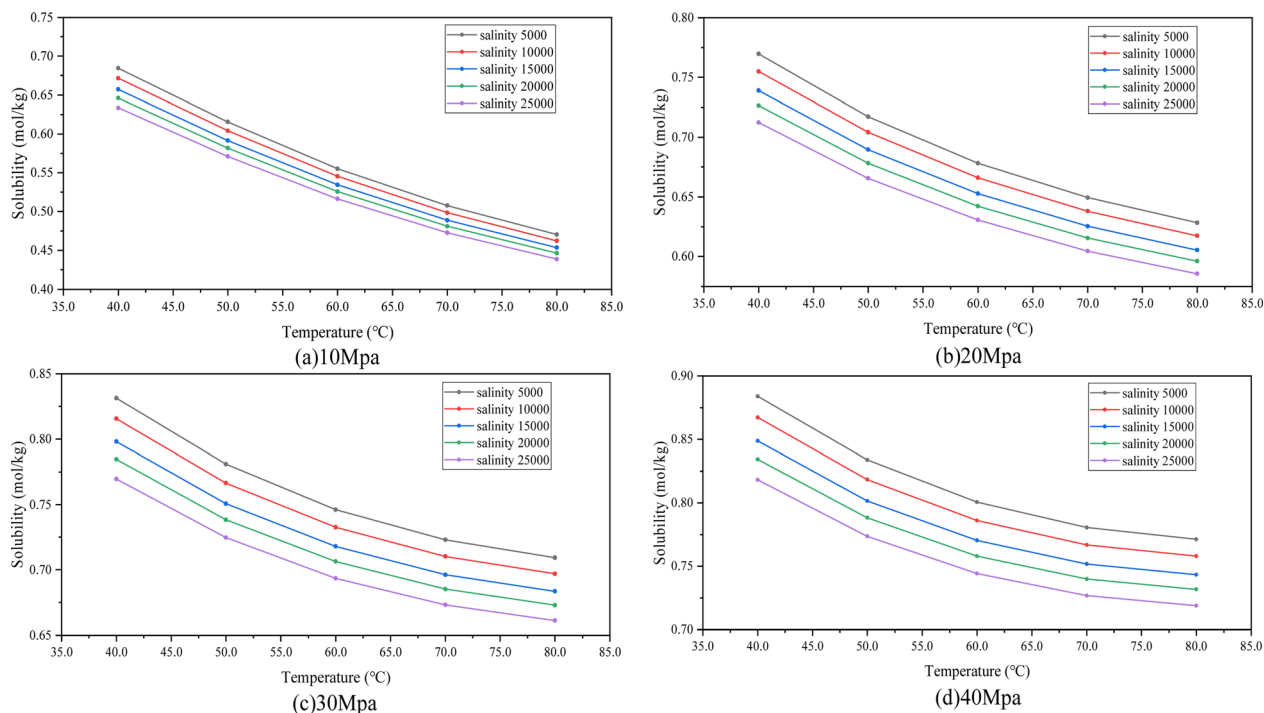
Fig. 12 The effect of temperature on CO_2 solubility in water at different pressures: (a) 10 MPa, (b) 20 MPa, (c) 30 MPa, (d) 40 MPa.
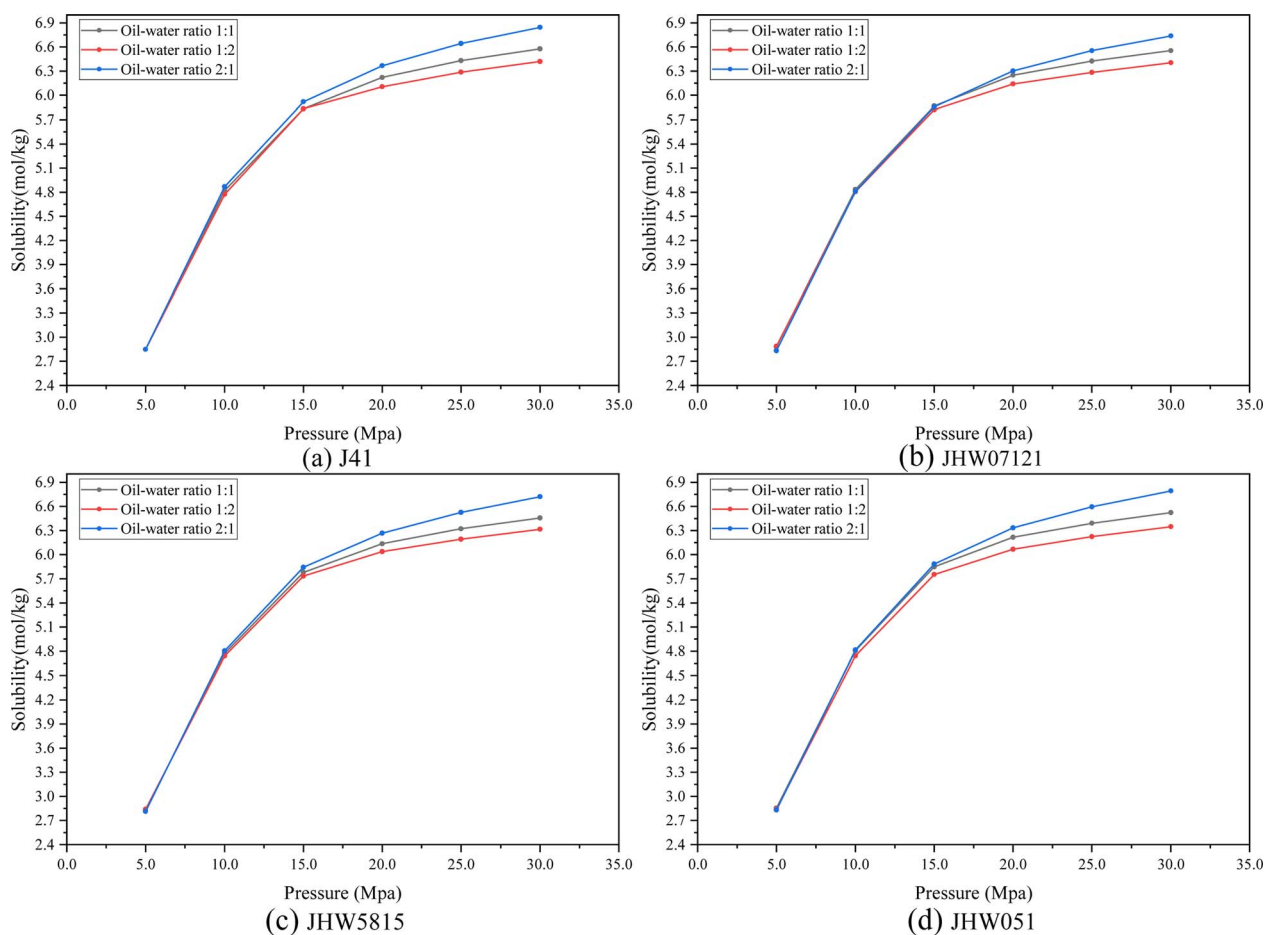

Fig. 13 The effect of oil–water ratio on the solubility of CO_2 in oil–water mixture: (a) J41, (b) JHW07121, (c) JHW5815, (d) JHW051.
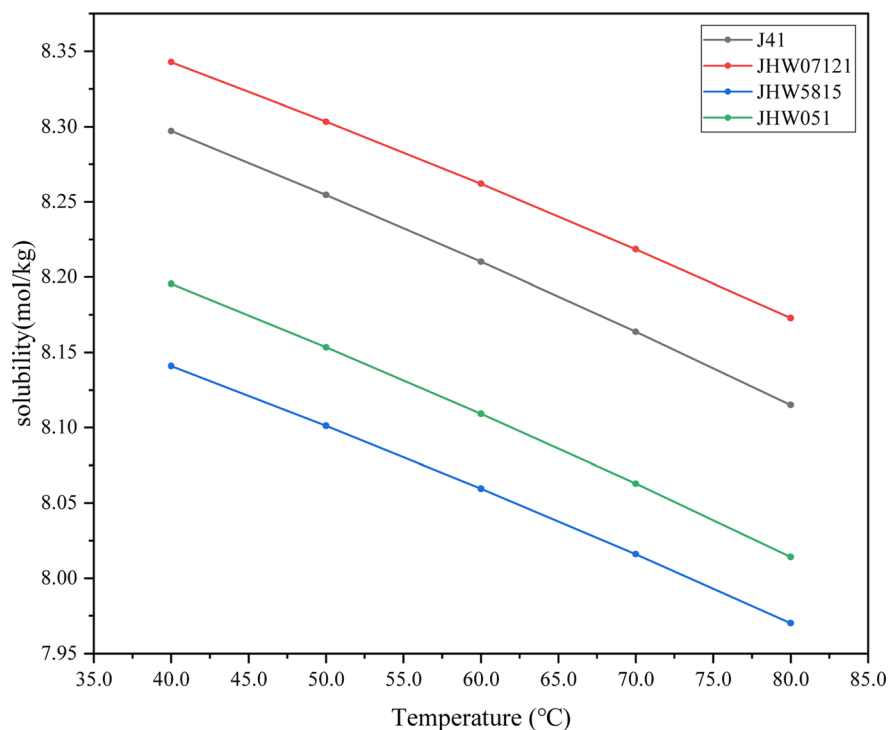
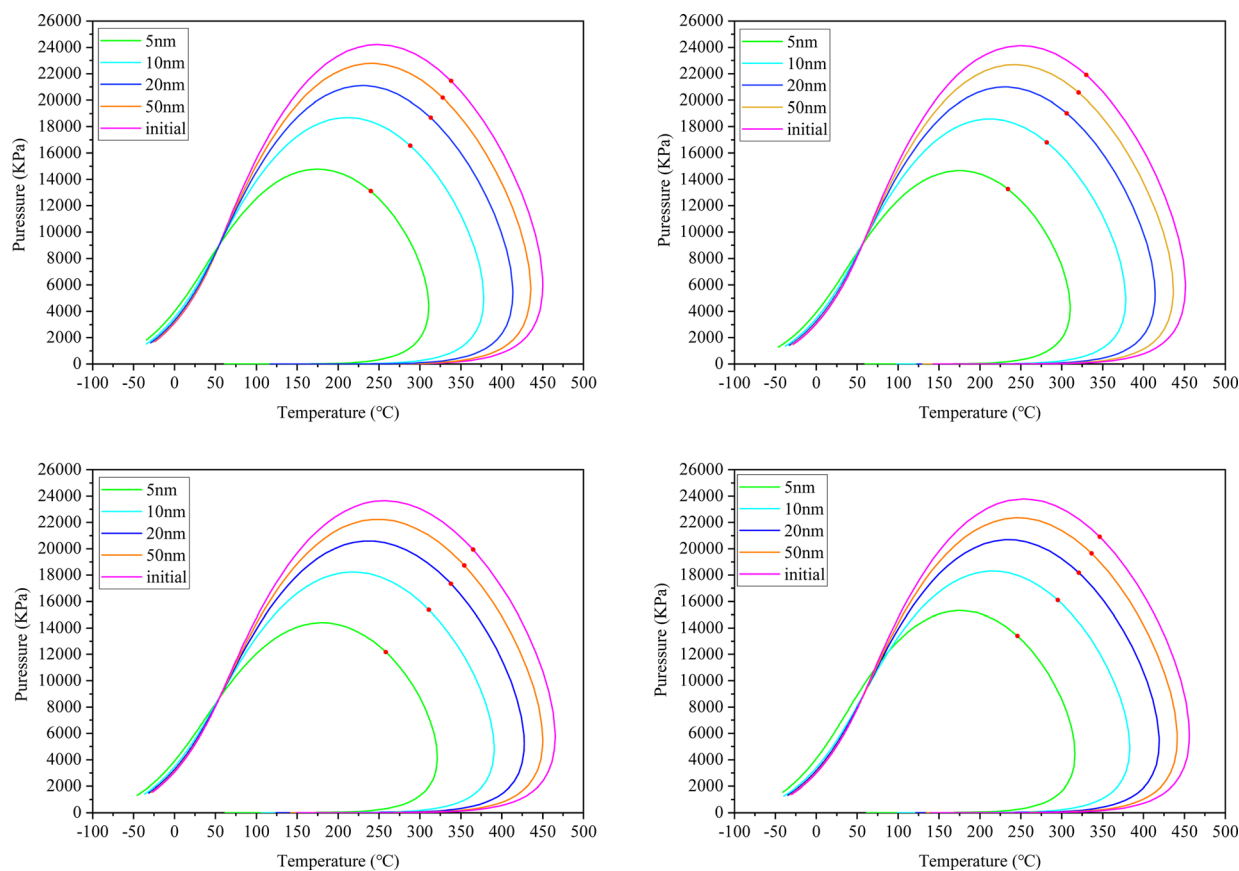**Fig. 14** CO_2 solubility in different oil–water mixtures.

Fig. 15 Phase envelope of four different crude oils at different pore sizes.

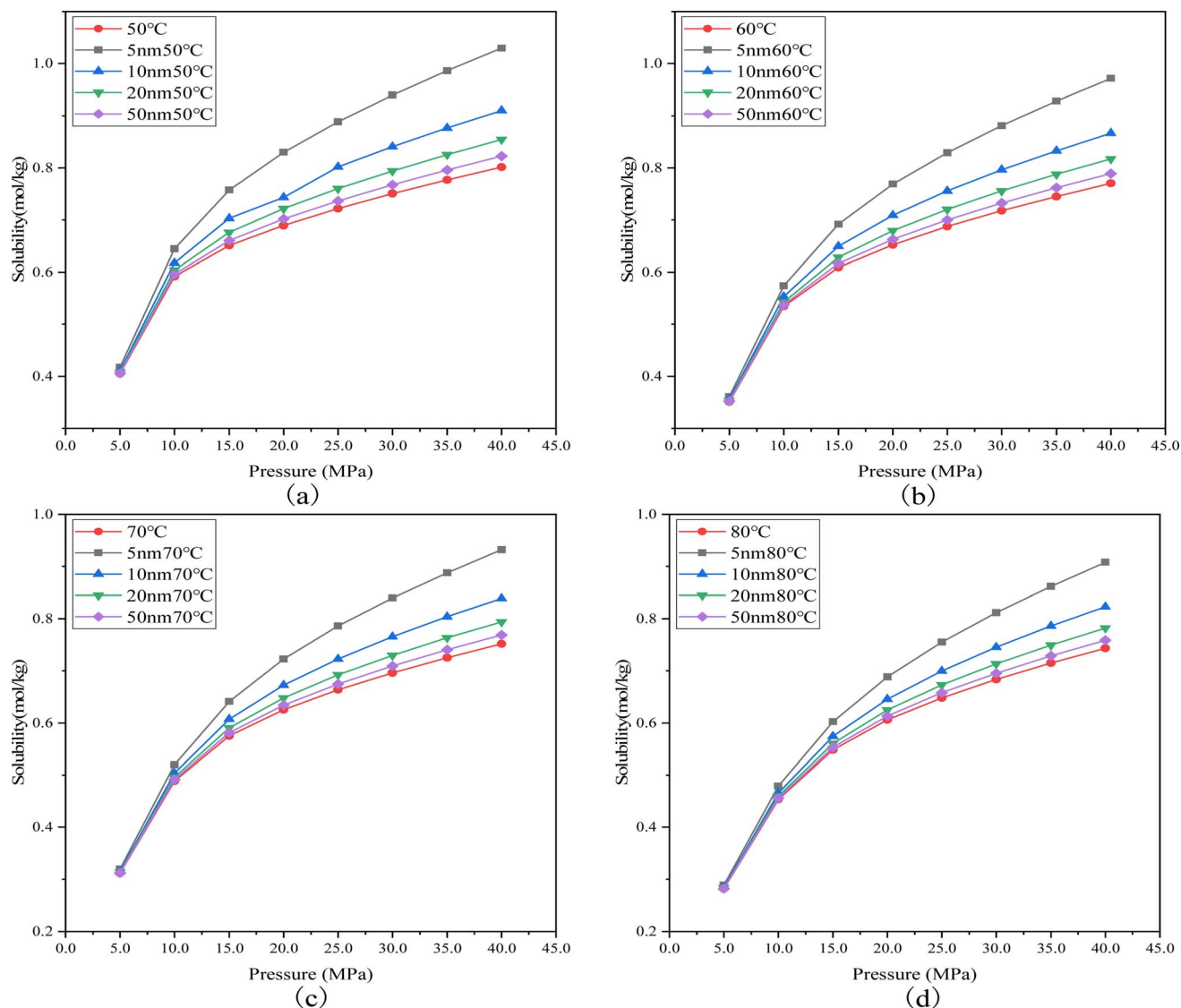© 2024 The Author(s). Published by the Royal Society of Chemistry

Fig. 16 The effect of nano-pore size on CO_2 solubility in water at different temperatures: (a) 50 °C, (b) 60 °C, (c) 70 °C, (d) 80 °C.

water mineralization on the solubility of CO_2 was more obvious under high pressure.

Elevated pressure increases the density of gas molecules and the frequency of collisions between gas molecules and solvent molecules, which is conducive to the dissolution of CO_2. An increase in temperature accelerates the movement of solvent molecules, leading to an increase in the frequency of collisions, the gas molecules are surrounded by solvent molecules at a slower rate, and solubility is consequently reduced. Since CO_2 dissolves in water mainly in ionic form, when the mineralization of the formation water is greater, the ionic concentration in the water is higher, leading to a decrease in CO_2 solubility.

It can be concluded that the solubility of CO_2 in water is affected by reservoir pressure, reservoir temperature and formation water salinity.

3.2.2 Solubility analysis of CO_2 in oil–water mixture. Fig. 13 shows the effect of oil–water ratio on CO_2 solubility in different oil–water mixtures at 2 : 1, 1 : 1 and 1 : 2 oil–water ratios. The influence of pressure on the solubility of CO_2 follows the similar

trend as CO_2 solubility in water. With the increase of injection pressure, the solubility of CO_2 in oil–water mixture increases as well. When the oil–water ratio is 2 : 1, the solubility of CO_2 in the oil–water mixture is the highest. When the oil–water ratio is 1 : 2, the solubility of CO_2 is the lowest. It is preferably for CO_2 to be dissolved in shale oil than water.

Fig. 14 shows the variation of CO_2 solubility with temperature in four different oil and water mixtures. It can be seen that the solubility of CO_2 in the oil–water mixture decreases with the increase in temperature. Results indicate that the solubility of CO_2 in the oil–water mixture is mainly affected by temperature, pressure and oil composition.

3.3 Solubility and phase state analysis of CO_2 under nanometer conditions

Fig. 15 compares the phase envelopes corresponding to different pore apertures. The phase behavior of fluids in shale reservoirs is difficult to obtain through direct experimental methods. To
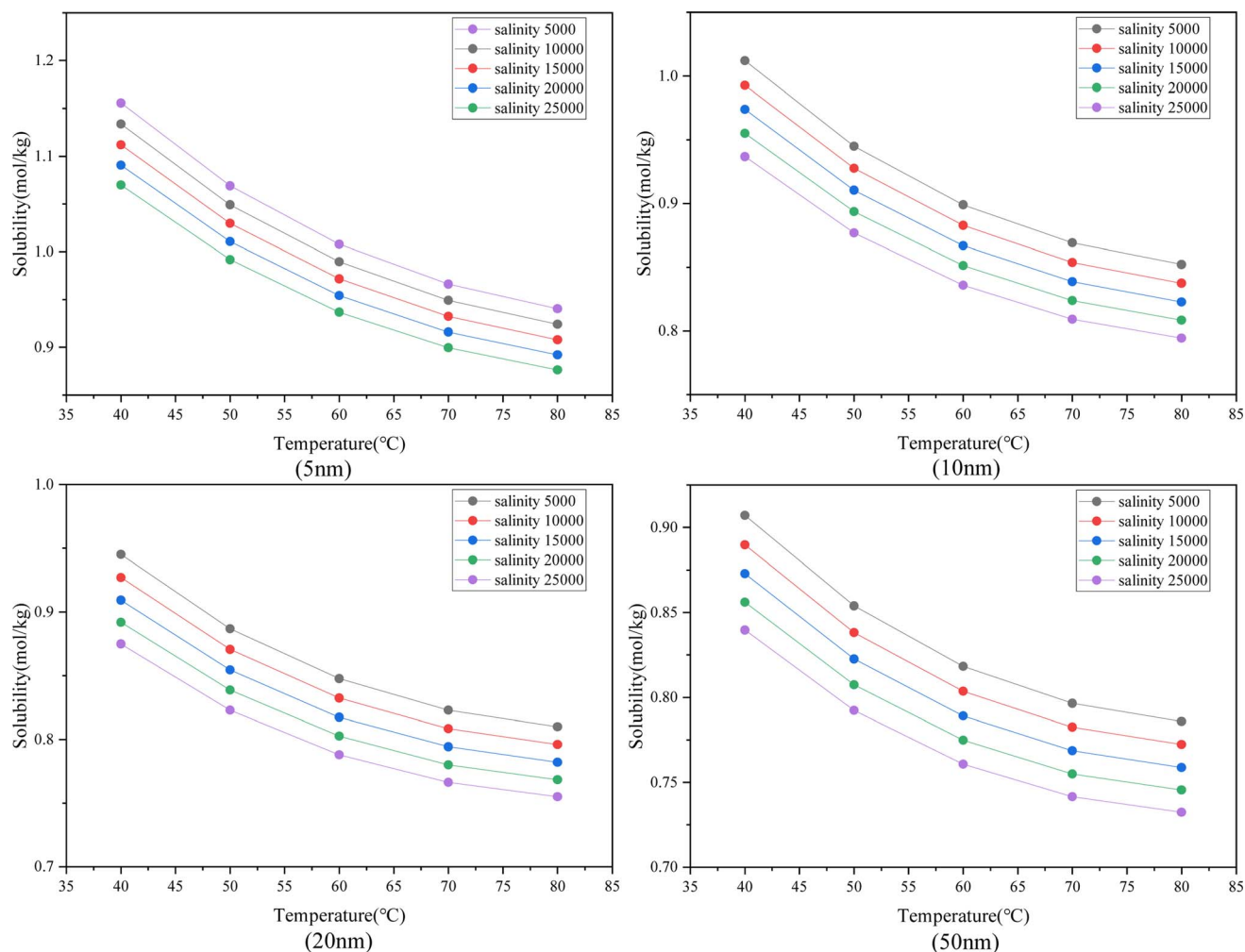
Fig. 17 The solubility of CO_2 in water varies with salinity under different pore sizes.

elucidate the influence of pore wall interaction on fluid phase behavior in nano-pores of shale reservoirs, the critical properties of fluid components confined at 5 nm, 10 nm, 20 nm, 50 nm were calculated by preceding method in Table 4. It can be seen from Fig. 15 that the phase envelope shrinkage is the largest when the pore aperture is at 5 nm. The strong surface–fluid interaction in the confinement pore space substantially shrinkage the P–T phase envelope from the bulk state.

The effect of nano-pore size on CO_2 solubility in water is shown in Fig. 16. Simulation results indicate that the pore confinement effect contributes to an increase of CO_2 solubility in water phase. Smaller pore sizes lead to a confined P–T phase envelope, thus the bubble point pressure of CO_2 injection was reduced. More volume of CO_2 can be dissolved in reservoir fluid compared to bulk state because of confined P–T envelope. It can be seen from Fig. 16 that under the same temperature and pressure, when the pore aperture is smaller, the solubility of CO_2 is higher.

The effect of salinity on solubility of CO_2 in water under different pore sizes at 40 MPa is shown in Fig. 17. Briefly, the trend of CO_2 solubility decreases with an increase of temperature and salinity. An increase of water salinity results in a reduction of CO_2 solubility in water. Under the same salinity,

when the reservoir temperature is higher, the solubility of CO_2 in water is lower. From results shown in Fig. 17, when the pore aperture is smaller, the solubility of CO_2 in water is higher.
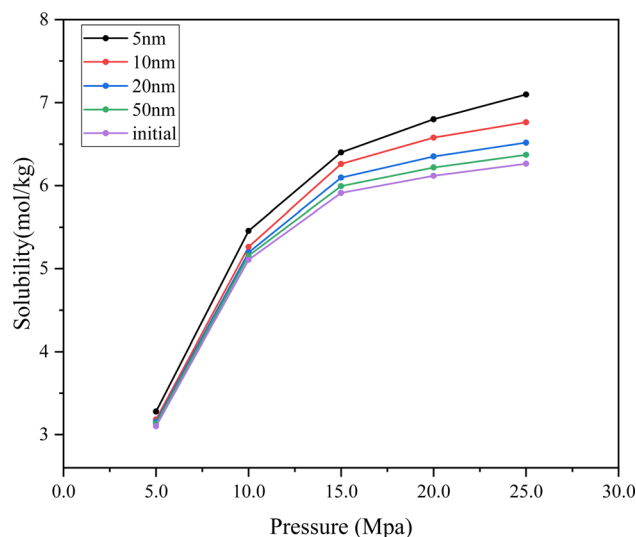

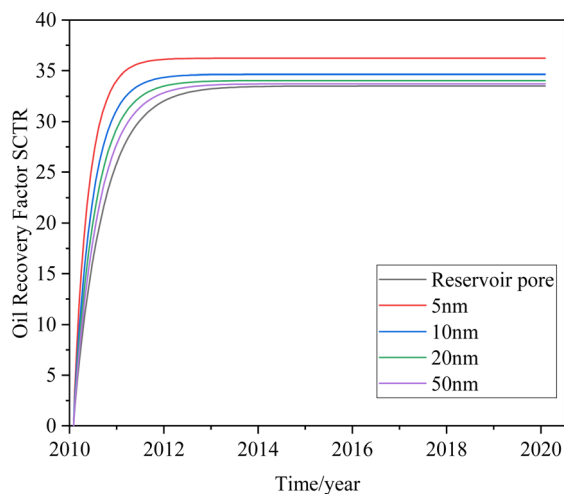**Fig. 18** The effect of pore sizes on CO_2 solubility in crude oil.

Fig. 19 Crude oil recovery degree at different pore sizes.

In comparison, the changes of CO_2 solubility in crude oil with different pore sizes is shown in Fig. 18. It can be seen that the solubility of CO_2 in crude oil increases with the increase of pressure. From results in Fig. 16–18, the overall trend of CO_2 solubility increases with the decrease of pore sizes. The reduction of pore size to nano-scale contributes to forming mixture of oil and CO_2, but when the pore size is smaller than the length of crude oil molecules, CO_2 molecules are less likely to interact with crude oil in the pores. Competitive adsorption of CO_2 and oil molecules at the pore wall where CO_2 strip the light oil molecules off the shale surface, it leads to the encapsulation of CO_2 molecules in the oil phase, which improves the dissolution of CO_2 to oil phase. The solubility of CO_2 in water and oil is affected by temperature, pressure, water salinity and pore sizes. By comparing CO_2 solubility in crude oil and water, the solubility of CO_2 in crude oil is much higher than water. It indicates that the storage of CO_2 in solution state primarily consisted in oleic phase.

It has been shown in the literature that the nano-restriction effect can reduce the light hydrocarbon extraction coefficient, which is conducive to the full contact of CO_2 with crude oil. Therefore, the nanopore restriction effect can improve the crude oil recovery to some extent. From Fig. 19 it can be seen that the highest degree of crude oil recovery is achieved when the nanopore size is 5 nm, which indicates that nanopores are favorable for CO_2 oil drive. It can be known that the solubility of CO_2 in the formation fluid decreases with the increase of nanopore size, and CO_2 drives the crude oil mainly by extracting the light components therein and thus reduces the viscosity of the crude oil, and the higher the solubility of CO_2 in the crude oil, the higher the efficiency of extracting the components of the crude oil and thus improves the efficiency of the oil drive.

4 Conclusion

In this study, the phase behavior of CO_2–water oil experiments was carried out to provide the key parameters for numerical simulation. In addition, numerical simulations were performed to investigate the influencing factors of CO_2 solubility in different reservoir fluids. The dissolution of CO_2 in interstitial water, crude oil and oil–water mixture was simulated. The effect of nano-pore confinement on the solubility of CO_2 was analyzed.

(1) A component model that can reflect the real fluid in the reservoir is obtained by phase fitting based on the experimental data, which provides a component basis for the subsequent establishment of the CO_2 oil drive model. It is found that the nanopore restriction will make the critical nature of the components smaller, which can lead to the contraction of the phase envelope. The smaller the nanopore diameter, the larger the contraction amplitude, the smaller the bubble point pressure of the system, and the smaller the minimum mixing pressure, so that CO_2 and crude oil can reach the mixing phase more easily, which can effectively improve the oil driving efficiency.

(2) The solubility of CO_2 in formation water, crude oil and oil–water mixtures is proportional to pressure and inversely proportional to temperature. It is found that the solubility of CO_2 in water is also related to the mineralization of formation water, which shows that the greater the mineralization of water, the lower the solubility of CO_2; The solubility of CO_2 in oil–water mixtures is also affected by the composition of the liquid phase, and the rule of change is that the larger the oil–water volume ratio is, the larger the CO_2 solubility is.

(3) Nanopores have a certain effect on the solubility of CO_2 in the formation fluid, the smaller the nanopore diameter, the greater the solubility of CO_2.

Abbreviation

P_{cb}	Critical pressure of the bulk fluid, atm
P_{cp}	Critical pressure of the confined fluid, atm
T_{cb}	Critical temperature of bulk fluid, K
T_{cp}	Critical temperature of confined fluid, K
r_p	Pore throat radius, nm
σ_{LJ}	Lennard-Jones size parameter, nm
V_e	Volume of fluids at equilibrium
V_l	Volume of liquid at equilibrium
$V_e–V_l$	Volume of gaseous CO_2 at equilibrium
P_0	Pressure of CO_2 at initial condition
P_e	Pressure at equilibrium condition;

Data availability

The data that supports the findings of this study are available within the article.

Conflicts of interest

There are no conflicts to declare.

Acknowledgements

References

1 L. Wang L, Y. Tian and X. Yu, Advances in improved/enhanced oil recovery technologies for tight and shale reservoirs, *Fuel*, 2017, **210**, 425–445.

2 K. Enab and H. Emami-Meybodi, Effects of diffusion, adsorption, and hysteresis on huff-n-puff performance in ultratight reservoirs with different fluid types and injection gases, *Energies*, 2021, **14**(21), 7379.

3 A. Fatah, Z. Bennour, Z. Mahmud, R. Gholami and M. Hossain, A review on the influence of CO_2/shale interaction on shale properties: Implications of CCS in shales, *Energies*, 2020, **13**(12), 3200.

4 S. Fakher, H. Abdelaal, Y. Elgahawy and A. El-Tonbary, *A Review of Long-Term Carbon Dioxide Storage in Shale Reservoirs*, SPE/AAPG/SEG Unconventional Resources Technology Conference, 2020.

5 S. Fakher and A. Imqam, A data analysis of immiscible carbon dioxide injection applications for enhanced oil recovery based on an updated database, *SN Appl. Sci.*, 2020, **2**, 448.

6 T. Wan and Z. J. Mu, The use of numerical simulation to investigate the enhanced Eagle Ford shale gas condensate well recovery using cyclic CO2 injection method with nano-pore effect, *Fuel*, 2018, **233**, 123–132.

7 R. Heller and M. Zoback, Adsorption of methane and carbon dioxide on gas shale and pure mineral samples, *Journal of Unconventional Oil and Gas Resources*, 2020, **8**, 14–24.

8 Z. Jin and A. Firoozabadi, Thermodynamic modeling of phase behavior in shale media, *SPE J.*, 2016, **21**(01), 190–207.

9 Y. B. Jiang, Experiment and characterization of porous media on Phase State of CO_2 injected crude oil, *Reservoir evaluation and development*, 2020, **10**(3), 23–27.

10 J. P. Welker, Physical properties of carbonated oils, *J. Pet. Technol.*, 1963, **15**(08), 873–876.

11 R. T. Suo, *Effect of CO_2 Phase and Purity in Different Cores on Residual Water in CO_2 Geologic Storage*, Inner Mongolia: Inner Mongolia University, 2021.

12 S. Luo, J. L. Lutkenhaus and H. Nasrabadi, Effect of Nano-Scale Pore Size Distribution on Fluid Phase Behavior of Gas IOR in Shale Reservoirs, In *SPE Improved Oil Recovery Conference*, 2018.

13 S. Verdier, H. Carrier, S. I. Andersen and J. L. Daridon, Study of Pressure and Temperature Effects on Asphaltene Stability in Presence of CO_2, *Energy Fuels*, 2006, **20**, 1584–1590.

14 B. Nojabaei, R. T. Johns and L. Chu, Effect of capillary pressure on phase behavior in tight rocks and shales, *SPE Reservoir Eval. Eng.*, 2013, **16**(03), 281–289.

15 G. L. Sheng, H. Zhao and Y. Su, An analytical model to couple gas storage and transport capacity in organic matter with noncircular pores, *Fuel*, 2020, **268**, 117288.

16 Y. L. Song, Z. J. Song and J. Guo, Phase Behavior and Miscibility of CO2–Hydrocarbon Mixtures in Shale Nanopores, *Ind. Eng. Chem. Res.*, 2021, **60**(14), 5300–5309.

17 B. A. Lopez, G. Hernandez and B. Czernia, Effects of thermodynamic and rock properties on the performance of liquids-rich nano-porous shale reservoirs, In *SPE Argentina Exploration and Production of Unconventional Resources Symposium*, 2018.

18 G. J. Zarragoicoechea and V. A. Kuz, Critical shift of a confined fluid in a nanopore, *Fluid Phase Equilib.*, 2004, **220**(1), 7–9.